Water Science & Technology

IWA PUBLISHING

Water Science & Technology Vol 85 No 9, 2748 doi: 10.2166/wst.2022.142

Adsorptive removal of methylene blue dye from aqueous streams using photocatalytic CuBTC/ZnO chitosan composites

Shreyas S. Dindorkar[a,†], Raj Vardhan Patel [b,†] and Anshul Yadav [b,*]

[a] Department of Chemistry, Jai Hind College, Mumbai 400020, India
[b] Membrane Science and Separation Technology Division, CSIR-Central Salt & Marine Chemicals Research Institute, Bhavnagar 364002, India
*Corresponding author. E-mail: anshuly@csmcri.res.in
†Equal contribution.

RVP, 0000-0003-1309-1573; AY, 0000-0003-1380-2662

ABSTRACT

In this study, a CuBTC/ZnO chitosan composite was synthesized for the adsorptive removal of methylene blue dye from aqueous streams. Characterization techniques, namely, scanning electron microscopy, Brunauer-Emmett-Teller, Fourier transform infrared, X-ray diffraction, and thermogravimetric techniques, were used to characterize CuBTC, ZnO, and CuBTC/ZnO chitosan composites. The scanning electron microscopy images revealed the rough and porous structures of the CuBTC/ZnO chitosan composite. The composites were tested for the adsorption capacity and removal efficiency towards the methylene blue dye by varying adsorbent dosage, adsorbate concentration, pH, and contact time. The pseudo-second-order and Langmuir models were the best fit for the adsorption of methylene blue on CuBTC/ZnO chitosan composite beads, indicating that the adsorption was monolayer and chemical in nature. The equilibrium dose of the composites was 1.6 g $L^{-1,}$ and the contact time was 90 min with a removal efficiency of 98.75%. The maximum adsorption capacity was 50.07 mg g^{-1}. Regeneration of the composites was performed to check the reusability of the synthesized CuBTC/ZnO chitosan composite beads. The active oxygenated species generated by the photocatalytic action of ZnO on the contaminated water was responsible for the degradation of methylene blue. The reported composite beads can be used for up to 5 cycles to remove methylene blue.

Key words: adsorption, CuBTC, methylene blue dye, photocatalysis, regeneration, ZnO

HIGHLIGHTS

- Photocatalytic CuBTC/ZnO chitosan composite beads were synthesized for adsorptive removal of methylene blue dye.
- The adsorption efficiency of the composite for the removal of methylene blue was investigated by varying reaction parameters such as contact time, dosage, initial concentration, and pH.
- The reported adsorbent could be used for up to 5 cycles to remove methylene blue without significant loss of removal efficiency.

GRAPHICAL ABSTRACT

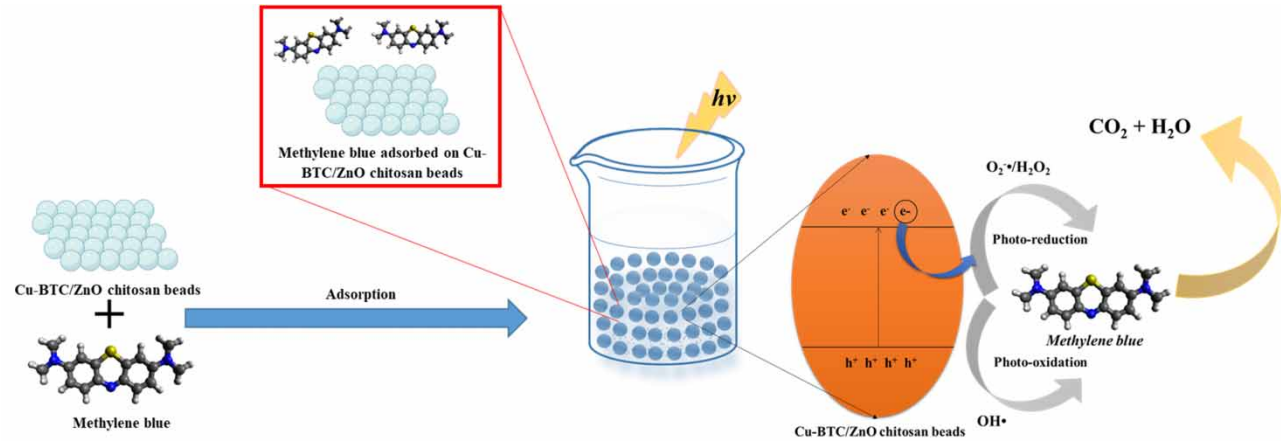

1. INTRODUCTION

Dyeing, one of the most energy-intensive operations carried out in the textile sector, has expanded rapidly in the past few decades. With growing urbanization, the demand for textile goods and products has increased, leading to extensive growth of dyeing industries. As a result of industrial operations and activities, the textile industry wastewater has started concentrating the water bodies with various hazardous and toxic substances such as dyes, by-products, heavy metals etc. (Pattnaik *et al.* 2018; Shindhal *et al.* 2021). Dyes have been identified as one of the major contaminants and toxicants in water bodies and are linked with toxicity, and have highly negative environmental repercussions if not removed from the water bodies for a longer period (Bangari *et al.* 2021; Yadav *et al.* 2021a). Methylene blue dye, for example, is an azo dye that poses serious hazards to human health if exposed to a large quantity (Bangari *et al.* 2022b; Yadav & Dindorkar 2022). Methylene blue dye has highly toxic effects on the intravenous route and releases toxic gases like nitrogen dioxide on combustion and is also responsible for irritation of the eyes and nausea when it comes in direct contact with the body (Shakoor & Nasar 2017; Yadav *et al.* 2021b). The major challenge in removing these toxic dyes is the additional stability imparted to them during the synthetic process. They need to be retained on the fabric for a longer time and in a variety of conditions. This makes it difficult to design strategies for effective removal (Imran *et al.* 2015).

Various methods have been developed for removing toxic dyes from water sources, such as photodegradation, coagulation-flocculation, advanced oxidation processes, biodegradation, membrane techniques, filtration, and ion exchange (Yaseen & Scholz 2019; Yadav *et al.* 2022b). However, most treatment processes (filtration, ion exchange, photodegradation) involve tedious setup, complex chemical analysis, and huge expenses and are time-intensive, making it difficult to implement these strategies commercially (Dindorkar *et al.* 2022; Yadav *et al.* 2022a). Adsorption is a comparatively simple, cost-effective and easy to design process. The metal-organic frameworks (MOFs), because of their porous nature, semiconductor-like behaviour, and flexible structures, are among promising candidates for water treatment and have shown promising photocatalytic activity (Hussain *et al.* 2018). Among MOFs, the most popular and most investigated MOF so far is [copper(ii)-benzene-1,3,5-tricarboxylate] (CuBTC) due to its high thermal stability and well-defined structure (Peedikakkal & Aljundi 2020). Therefore, CuBTC may be favourable for the removal of dyes from wastewater. The adsorption using MOFs shows a great capacity in removing dyes from the water. Rajak *et al.* (2017) reported a novel cobalt-based MOF for the adsorption of Chicago sky blue and Congo red dyes. Liu *et al.* (2020) synthesized a poly threaded Mn^{II}-MOF based on a tridentate N-containing ligand that showed high adsorption capacity for methyl orange. Shahnawaz Khan *et al.* (2020) reported the factors that trigger the dye adsorption on MOFs. Mariyam *et al.* (2020) performed a topological analysis of tetrazole-based MOFs and examined their dye adsorption properties against methylene blue. However, it is evident from the reports that the MOF-based photocatalytic materials' regeneration studies after the first cycle of degradation are insufficient and lack evidence of regeneration (Zhao *et al.* 2017; Zhang *et al.* 2018). The major problem with adsorption is the reusability of adsorbents as the adsorbents get poisoned as the active sites get blocked. Zinc oxide (ZnO) is a well-known material that exhibits photocatalytic properties and

can be used to regenerate adsorbents (Adeel *et al.* 2021). Cai *et al.* (2022) found that surface area and photocatalytic properties increased after incorporating ZnO in waste pine.

Despite having known the potential of CuBTC in the adsorption of dyes, their studies remained restricted. Moreover, very few reports are available wherein the attempts are made to design CuBTC-based composites that can adsorb the dyes and degrade them to less harmful products. This study used CuBTC and chitosan and photoactive ZnO nanoflowers to synthesize photocatalytic CuBTC/ZnO chitosan composites. The composite material was investigated for its efficiency to adsorb methylene blue from the aqueous streams. The composite beads were characterized using scanning electron microscopy (SEM) to analyze their morphological properties, X-ray diffraction (XRD) and Fourier transform infrared spectra (FT-IR) to gain insights into their structural properties, Brunauer-Emmett-Teller (BET) analysis to determine their surface area and thermogravimetric analysis (TGA) to study their thermal stability. The adsorption isotherms and the kinetic models were used to establish the regeneration mechanism. The regeneration studies of the CuBTC/ZnO chitosan composite for the photocatalytic degradation of the methylene blue dye under solar irradiation were also performed.

2. MATERIALS AND METHODS

2.1. Materials

Copper nitrate ($Cu(NO_3)_2$), zinc acetate dihydrate ($Zn(CH_3COO)_2.2H_2O$), chitosan polymer, trimesic acid (H_3BTC), dimethylformamide (DMF), methylene blue dye, ethanol, and sodium hydroxide (NaOH) were procured from SRL chemicals. The solvent system chosen for the adsorption experiments was deionized water and obtained from Millipore Q BIOCEL unit, Millipore.

2.2. Synthesis of CuBTC, ZnO nanoflowers, and CuBTC/ZnO chitosan composite beads

CuBTC was prepared by the method reported earlier (Xu *et al.* 2016). The solvothermal synthesis of CuBTC involved the addition of 1.45 g $Cu(NO_3)_2$, 0.84 g H_3BTC, and 80 ml DMF in a 100 ml beaker and subsequent stirring till it was homogenous. The suspension was transferred to a stainless-steel autoclave and held at 140 °C for 24 h. After cooling to room temperature, the light blue crystalline product was washed with DMF and methanol several times and dried overnight at 50 °C.

ZnO nanoflowers were prepared by the method reported earlier (Patel & Yadav 2022). 0.2 M zinc acetate dihydrate was dissolved in deionized water at room temperature (~25 °C) followed by sonication for 2 h. A 0.02 M NaOH solution was prepared separately by dissolving the desired quantity of NaOH in deionized water. To the solution of 0.2 M zinc acetate dihydrate, the 0.02 M of NaOH solution was added dropwise with a constant stirring of 300 rpm. The resultant white precipitate was washed with ethanol multiple times. The filtered white precipitate was dried in a vacuum oven at 60 °C for 10 h to obtain ZnO nanoflowers.

CuBTC/ZnO chitosan composite beads were synthesized by the method reported earlier (Yadav *et al.* 2022c). The ionotropic gelation synthesis of CuBTC/ZnO chitosan composite beads involved the addition of CuBTC (500 mg) to 100 ml of deionized water and 100 mg of ZnO nanoflower followed by magnetic stirring for 10 min. 2 g chitosan and 2% w/v acetic acid were added to the solution and stirred until a homogeneous solution formed. Spherical beads of the solution were then dropped into 1 N NaOH solution using a syringe and incubated in the basic solution overnight at room temperature. After incubation, the beads were filtered and washed several times with deionized water until the solution's pH became neutral.

2.3. Adsorption and regeneration experiments

The details on adsorption experiments are included in section S1, ESI.

2.4. Characterization techniques and instrumentation details

The details on characterization techniques are included in section S2, ESI.

3. RESULTS AND DISCUSSION

3.1. Characterization studies

The SEM images of as-synthesized CuBTC and ZnO nanoflowers are shown in Figure 1. The low magnification image of CuBTC showed that the units were individual with an octahedral geometry and did not agglomerate (Figure 1(a)). The

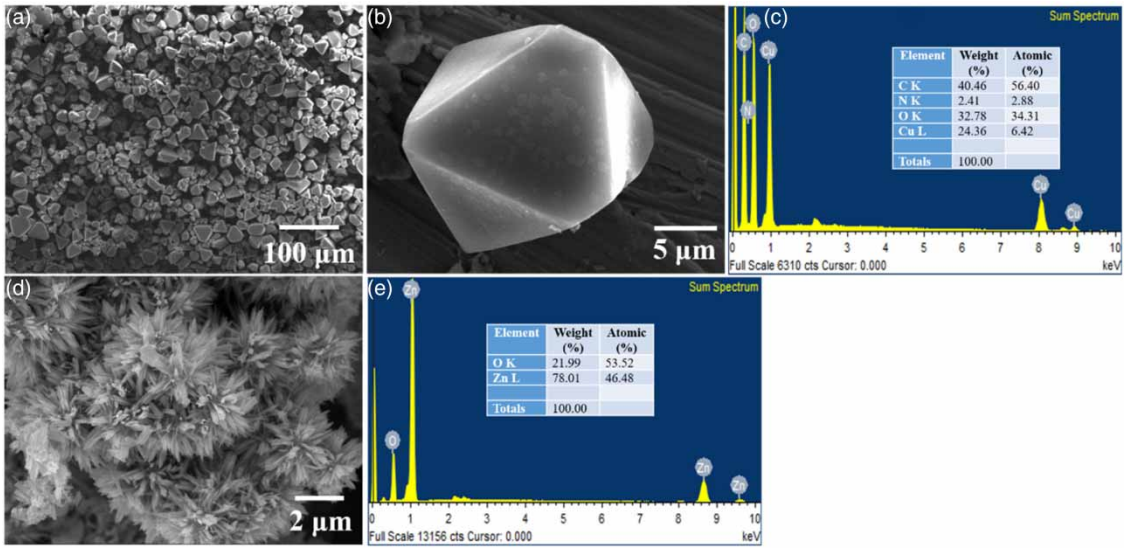

Figure 1 | SEM and EDS spectra of as-synthesized (a–c) CuBTC MOF particles (d, e) ZnO nanoflowers.

high=magnification image of a single CuBTC unit (Figure 1(b)) shows that these octahedral units were elongated along an axis. This distortion from regular geometry was attributed to the Jhan-Tellar distortion (Schäfer *et al.* 2017). Further, the atomic percentage of Cu, C, O, and N in CuBTC were 6.42, 56.40, 34.31, and 2.88, respectively. A high proportion of C and O and low proportions of N was attributed to the rich organic profile of the BTC ligand. The high-magnification image of the ZnO reveals its flower-like shape (Figure 1(e)). The smaller nanoflower structures agglomerated and gave rise to comparatively larger nanoflowers. The corresponding EDS spectra shown in Figure 1(f) demonstrate the atomic percentage of Zn (53.52%) and O (46.48%), respectively, in the synthesized ZnO nanoflowers. It is evident from the EDS plots that the as-synthesized ZnO nanoflowers were of high purity.

The SEM image of CuBTC/ZnO composite beads reveals the rough and porous surface (Figure 2(a) and 2(b)) and confirms the high purity of as-synthesized composite beads. The atomic percentages of Cu, C, O were 2.27%, 48.59%, and 39.60%, respectively (Figure 2(c)). The atomic percentage of nitrogen was 7.39% was due to the copper nitrate used for the synthesis. A negligible percentage of impurities (~2%) were found mainly due to the Si, Mg and Zn.

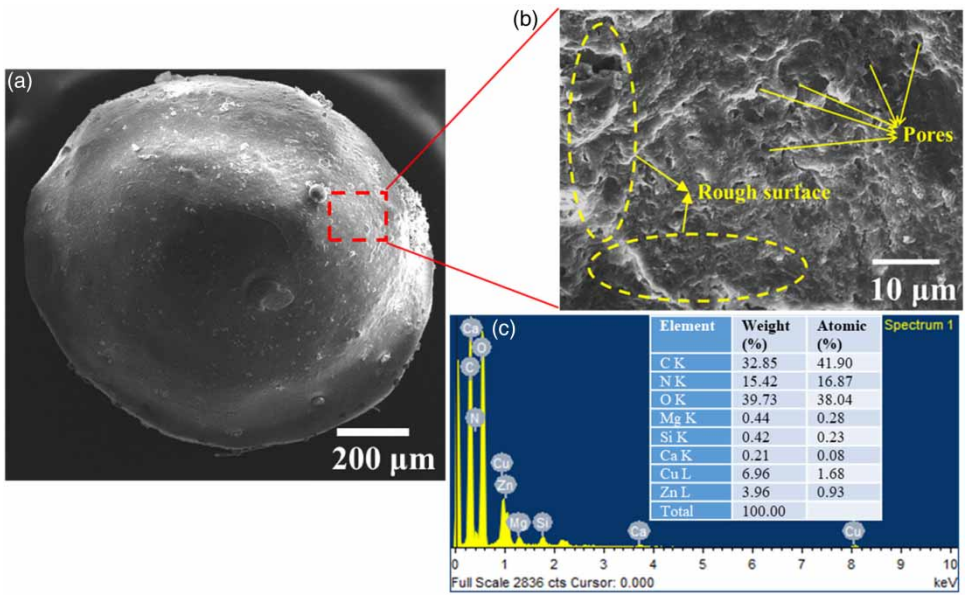

Figure 2 | SEM and EDS spectra image of as-synthesized CuBTC/ZnO chitosan composite beads.

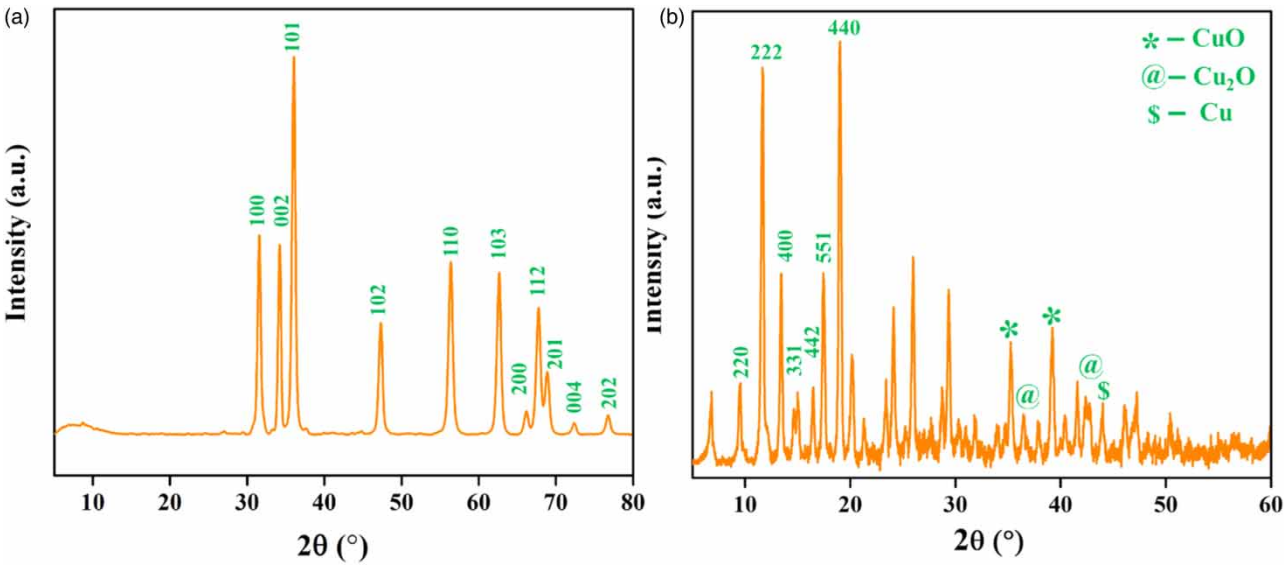

Figure 3 | XRD spectra of (a) ZnO nanoflowers and (b) CuBTC.

The XRD spectra of the ZnO nanoflowers, CuBTC, and the CuBTC/ZnO chitosan composite beads are depicted in Figure 3. The crystalline nature of the ZnO nanoflowers was confirmed from the XRD spectra. All the reflections were indexed to the wurtzite phase of ZnO (ICDD no. 36–1451). Two distinct characteristic peaks were observed for the CuBTC at 2θ values of 13.5° and 19.1°, respectively. Certain other peaks were also observed at higher 2θ values were due to CuO, Cu_2O and Cu. The XRD results for CuBTC and ZnO agreed with previous studies (Yedurkar *et al.* 2016; Cheng *et al.* 2018).

Figure 4(a) shows the FT-IR spectra of the synthesized ZnO nanoflowers. A sharp band at 488 cm^{-1} was due to Zn-O stretching. In octahedral coordination, the Zn-O stretchings were observed at 654 cm^{-1}. Strong tetrahedral coordinations confirmed the wurtzite structure of ZnO (Mohd Yusof *et al.* 2020). The band at 1,370 cm^{-1} was linked to the asymmetric stretching of C = O. At 2,855 cm^{-1} and 2,916 $cm^{-1,}$ bands arose due to C-H bending and C-H stretching vibrations, respectively. The FT-IR spectra of CuBTC are also shown in Figure 4(a). Due to Cu-O stretching, sharp bands appeared at 478 and 730 cm^{-1} (Arul & Abraham John 2017). A band at 1,106 cm^{-1} was ascribed to carboxylate stretching vibration. The bands that appeared between 1,450–1,350 cm^{-1} and 1,625–1,550 cm^{-1} were due to the asymmetric and symmetric stretching of carboxylate, respectively (Khoshhal *et al.* 2015). Figure 4(b) shows the FT-IR spectra of CuBTC/ZnO chitosan composite beads. The broad hump between 3,331 and 3,450 cm^{-1} was ascribed to –OH and -NH stretching vibrations (Li *et al.* 2016). The characteristic out of plane vibrations for chitosan were observed at 562 and 1,174 cm^{-1} (for the C–O–C stretching) due to the glucopyranose ring in chitosan polymer (Oh *et al.* 2019). At 1,589 cm^{-1}, a band corresponding to the N-H bending of the primary amine group was observed. The strong characteristic bands of the CuBTC were located at 1,646 cm^{-1}. A sharp band for Zn-O stretching in tetrahedral coordination was observed at 488 cm^{-1}.

To study the stability of the CuBTC and CuBTC/ZnO chitosan composite beads at high temperatures, TGA thermographs were obtained (Figure S1, ESI). A similar TGA trend was shown by both the composites. The composite bead without ZnO showed a steep decrease in mass composition, and around 800 °C, the majority of the composite beads (~80%) got decomposed. However, after incorporating the ZnO nanoflowers, improved results were seen. The TGA curves revealed a residual mass of around 84% near 300 °C, followed by a loss of about 40% mass up to 350 °C. A continuous loss of mass was observed due to the rich organic profile of the composite beads that is mainly due to chitosan and the BTC ligand.

The BET plots were obtained to investigate the surface area of the CuBTC/ZnO chitosan beads (Figure S2, ESI). The BET constant, C, was evaluated by the adsorption of nitrogen gas on the beads at 120 °C using the equation:

$$\frac{1}{Q\left[\left(\frac{P_0}{P}\right)-1\right]} = \frac{C-1}{Q_m C}\left(\frac{P}{P_0}\right) + \frac{1}{Q_m C} \quad (1)$$

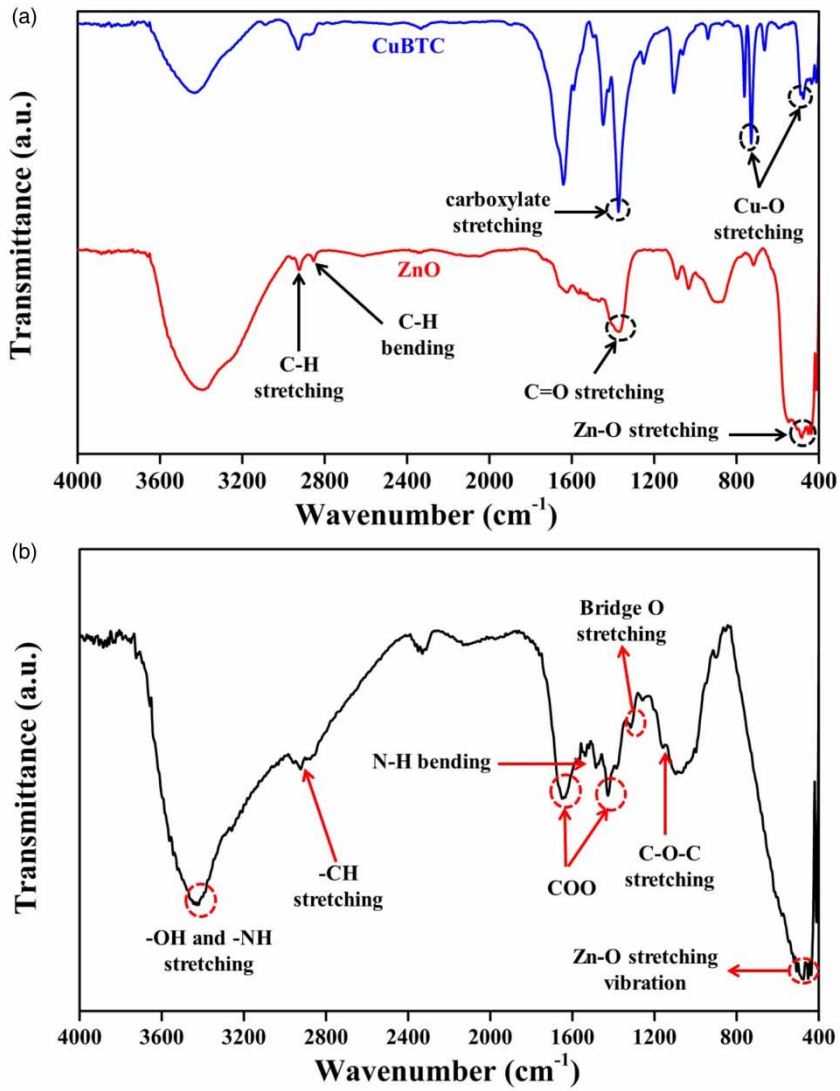

Figure 4 | FT-IR spectra of CuBTC/ZnO chitosan composite beads.

where P – equilibrium pressure, P_0 – saturation pressure, Q – the amount of gas adsorbed on the adsorbate, Q_m – monolayer adsorbed and C – BET constant. The BET plot of adsorbed volume against the relative pressure is shown in Figure 6(a). The isotherms were of type IV as per the IUPAC nomenclature (Sharma & Jha 2017). The type IV curve indicated the porous nature of the CuBTC/ZnO composite beads, a typical characteristic of mesoporous materials. Mesoporous materials are good adsorbents and hence methylene dye was well adsorbed at the surface of CuBTC/ZnO chitosan composite beads (Heidari *et al.* 2021). The BET constant was 105.627. The total surface area of 5.91 $m^2\ g^{-1}$ was obtained from the equation

$$S_{total} = \frac{Q_m N_S}{V} \tag{2}$$

where N is the Avogadro number and V is the volume of the adsorbate gas. The cumulative pore volume and pore size of $6.418 \times 10^{-4}\ cm^3\ g^{-1}$ and 21.73 Å, respectively, were obtained from Figure S2(b), ESI.

3.2. Adsorption experiments

3.2.1. Effect of dosage

The effect of the CuBTC/ZnO chitosan composite dose on adsorption and removal efficiency is depicted in Figure 5. The removal efficiency decreased with the dosage of adsorbent up to 1.6 g L^{-1}. This was attributed to the availability of more

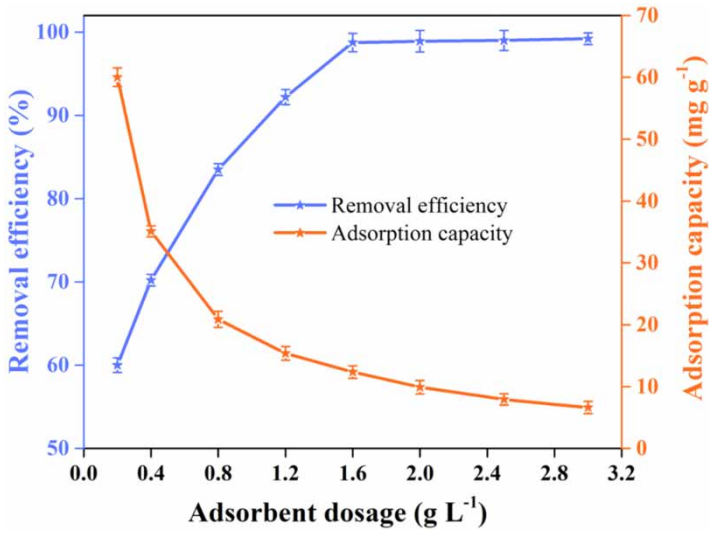

Figure 5 | Removal efficiency and adsorption capacity of CuBTC/ZnO chitosan composite beads with varying adsorbent dosage for methylene blue dye. (initial dye concentration: 20 ppm, contact time: 90 minutes, and pH: 7).

active sites for adsorption on increased dosage. An equilibrium value of 1.6 g L^{-1} was obtained, for which the adsorption capacity and the removal efficiency was maximum. The adsorption capacity decreased drastically in the initial stages, followed by a steady decrease. This increase in the adsorbent dose resulted in aggregation or overlapping of adsorption sites (Ndi Nsami & Ketcha Mbadcam 2013). As the adsorption experiments were carried out in polar aqueous media, the possibility of hydrogen bonding increased, which led to the agglomeration of the composites with an increase in dosage (Mahmoudzadeh *et al.* 2013).

3.2.2. Effect of initial concentration of methylene blue dye

Figure 6 revealed that when the initial concentration of the methylene blue dye was varied, the removal efficiency of around >98% was observed till the 60 ppm methylene blue dye concentration. A drastic decrease in removal efficiency was observed beyond 60 ppm methylene blue dye concentration. This was attributed to the increased concentration of methylene blue molecules and the same amount of adsorbent, meaning the number of active sites remained constant. Initially, when the

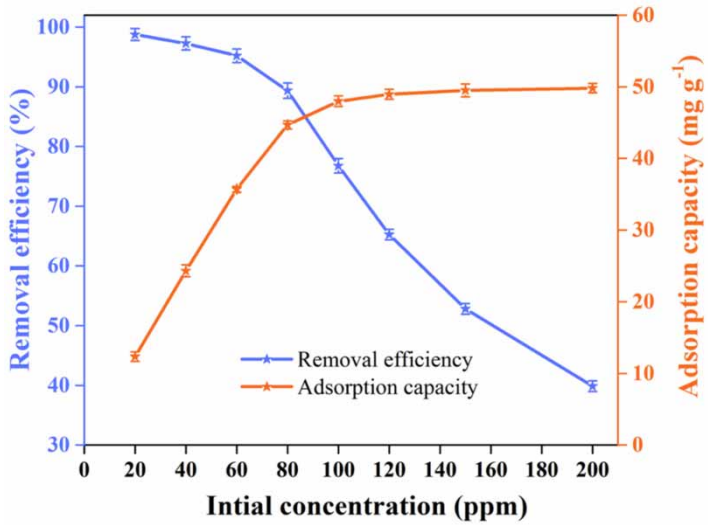

Figure 6 | Removal efficiency and adsorption capacity of CuBTC/ZnO chitosan composite beads with varying initial concentrations of methylene blue dye. (adsorbent dose: 1.6 g L^{-1}, contact time: 90 minutes, and pH: 7).

concentration of the methylene blue dye was 20 ppm, the adsorption capacity was around 10 mg g^{-1}. As the methylene blue dye concentration increased, the adsorption capacity rose to about 50 mg g^{-1} and remained constant.

3.2.3. Effect of pH

pH plays a crucial role in the adsorption of the dyes. The variations in the pH of the methylene blue dye solution affected the adsorption capacity and the removal efficiency of CuBTC/ZnO chitosan composite beads, as shown in Figure 7. As the pH increased, the adsorption capacity and the removal efficiency increased. The removal efficiency (~99%) and the adsorption capacity (12 mg g^{-1}) were maximum at the neutral pH. Hence, the neutral pH was considered optimum and maintained in the further batch adsorption experiments. At higher pH, methylene blue dye-containing chlorine anions react with NaOH to produce NaCl and methylene blue-S + OH (aqueous) through displacement reaction. NaCl salt decreases the adsorption of methylene blue-S + OH (aqueous) on the adsorbent surface (Amode *et al.* 2016).

3.2.4. Effect of contact time

Contact time refers to when the adsorbate molecules are in contact with the adsorbent. The more the contact time, the greater the chances of the adsorbate molecule to contact the adsorbent's active sites (Hao *et al.* 2021). From Figure 8, it was observed that the removal efficiency and the adsorption capacity increased with contact time. This was attributed to the fact that initially, more sites were available, and the number decreased during the adsorption process. An equilibrium value of 90 min was obtained where their removal efficiency reached ~100%.

The maximum adsorption capacity (q_m) of various adsorbents reported in the literature against methylene blue dye are compared in Table S1, ESI. Parameters such as adsorption capacity (q_m), adsorbent dose, pH and contact time formed the basis of the comparison. The results from the present study were comparable with previous works, suggesting that methylene blue could be easily adsorbed on the as-synthesized CuBTC/ZnO composite beads prepared in this work. The additional advantage over the other reported studies was the photocatalytic degradation under visible sunlight.

3.3. Adsorption kinetics

To propose a plausible kinetic mechanism of the adsorption process, adsorption kinetics was investigated based on pseudo-first-order (PFO) and pseudo-second-order (PSO) models. Table 1 depicts the adsorption capacities, kinetic coefficients, reduced chi-square, and residual sum of squares for PFO and PSO kinetics for adsorption of methylene blue dye on CuBTC/ZnO composite beads. The correlation coefficient (R^2) for PFO (0.9653) model deviated more from the unity value compared to the PSO (0.9968) model. The closeness of the R^2 value for the PSO model indicated that the non-linear second-order model fits well for the adsorption of methylene blue on CuBTC/ZnO chitosan beads. The better fitting of the PSO model confirmed that the adsorption was chemical in nature (Kuwer *et al.* 2021). PSO showed a lower value

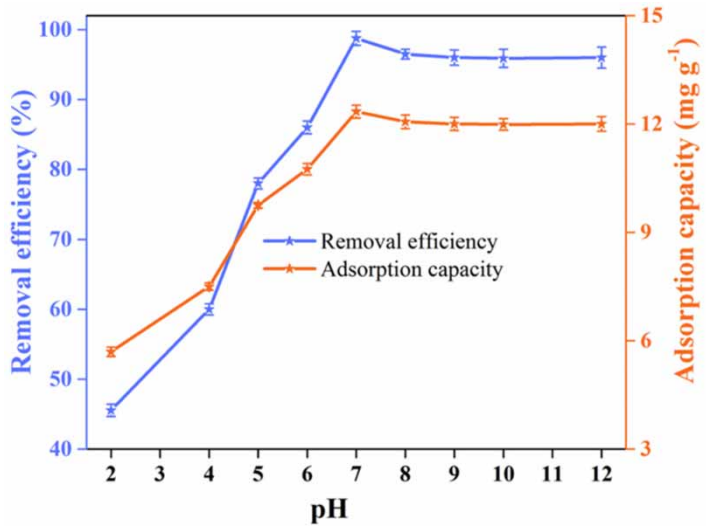

Figure 7 | Removal efficiency and adsorption capacity of CuBTC/ZnO chitosan composite beads with varying pH for methylene blue dye adsorption (adsorbent dose: 1.6 g L^{-1}, initial dye concentration: 20 ppm, and contact time: 90 minutes).

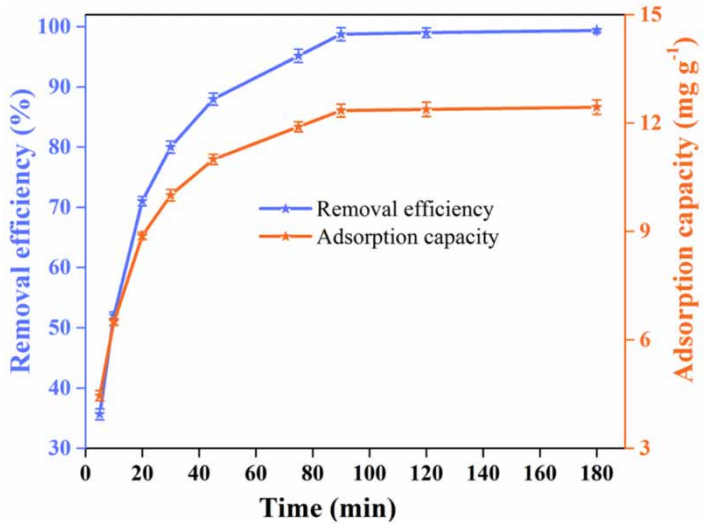

Figure 8 | Removal efficiency and adsorption capacity of CuBTC/ZnO chitosan composite beads with varying contact time for methylene blue dye. (adsorbent dose: 1.6 g L^{-1}, initial dye concentration: 20 ppm, and pH: 7).

Table 1 | Parameters of PFO and PSO kinetics for adsorption of methylene blue dye on CuBTC/ZnO composite beads

	PFO	PSO
q_e (mg g^{-1})	12.056	13.450
k ($min^{-1)}$	0.071	0.007
R^2	0.965	0.997
Reduced chi-square	0.286	0.026
Residual sum of squares	2.002	0.183

for the residual sum of the square and reduced chi-square than the PFO model. This suggested that the difference between the theoretical and experimental values for PSO and PFO was minimum. The initial adsorption of methylene blue was faster for PFO than PSO (Figure 9).

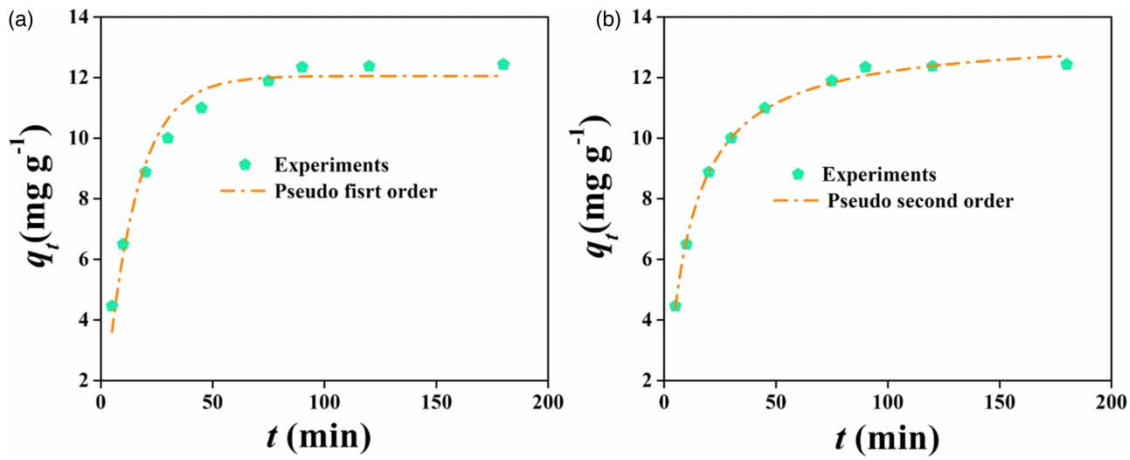

Figure 9 | Non-linear form of kinetic isotherms (a) PFO and (b) PSO.

3.4. Adsorption isotherms

The Freundlich and Langmuir isotherm models were used to investigate the adsorption of methylene blue dye on CuBTC/ZnO composite beads. The regression coefficient (R^2), reduced chi-square, and residual sum of squares were evaluated to differentiate between two isotherm models (Table 2). The R^2 value was close to unity in the case for the Langmuir model (Freundlich: 0.8036 and Langmuir: 0.9914), confirming that the Langmuir isotherm model fit. The Langmuir model gives a fraction of the surface covered by adsorbate molecules at a particular temperature and pressure. A typical Langmuir isotherm shows a characteristic horizontal asymptote indicating saturation after the monolayer adsorption. This indicated that the adsorption mechanism of methylene blue dye on CuBTC/ZnO chitosan composite beads was chemisorption (Bangari *et al.* 2022a). The closeness of experimental and predicted data points was also observed (Figure 10).

3.5. Plausible adsorption and degradation mechanism

To comment upon the removal of methylene blue dye by the CuBTC/ZnO chitosan composite beads, the role of the individual component in the composite must be studied. The BTC ligand or the benzene tricarboxylate ion of the CuBTC is rich in charge density due to the availability of π-electrons of the benzene ring and the carboxylate groups (Hu *et al.* 2015). The electron-rich profile of the ligand in the CuBTC makes the adsorption easier by attracting the cationic methylene blue dye molecule. Further, CuBTC has large octahedral cavities that facilitate adsorption. The methylene blue dye molecules are present at a higher rate constant than the single molecules. Chitosan, a sugar polymer, adsorbs the methylene blue dye molecules in aggregate form on its surface (Kellner-Rogers *et al.* 2019). Since the adsorption process follows the PSO model, methylene blue dye was adsorbed in aggregated form. Hence, CuBTC present in the CuBTC/ZnO chitosan composite beads is majorly responsible for providing the vacant sites for the adsorbed methylene blue dye molecules. In contrast, the chitosan provides a surface where the methylene blue molecules aggregated and adsorbed. The CuBTC/ZnO chitosan composite beads' degradation efficiency was tested to degrade methylene blue dye under solar irradiation. ZnO is well known for its photocatalytic activity and thus imparts photocatalytic properties to the CuBTC/ZnO composite beads (Biswal *et al.* 2021). ZnO has a semiconducting nature at room temperature with a bandgap of 3.37 eV (Razavi-Khosroshahi *et al.* 2017). Irradiating ZnO with sunlight is sufficient to promote the electrons from the filled valence band to the empty

Table 2 | Parameters of Freundlich and Langmuir isotherms for the adsorption of methylene blue dye on CuBTC/ZnO composite beads

Freundlich isotherm	K_F ((mg g^{-1}) (L mg^{-1})$^{-1/n}$)	1/n	R^2	Reduced chi-square	Residual sum of squares
	26.761	0.153	0.804	38.587	231.523
Langmuir isotherm	q_m (mg g^{-1})	K_L (L mg^{-1})	R^2	Reduced chi-square	Residual sum of squares
	50.069	0.941	0.991	1.682	10.089

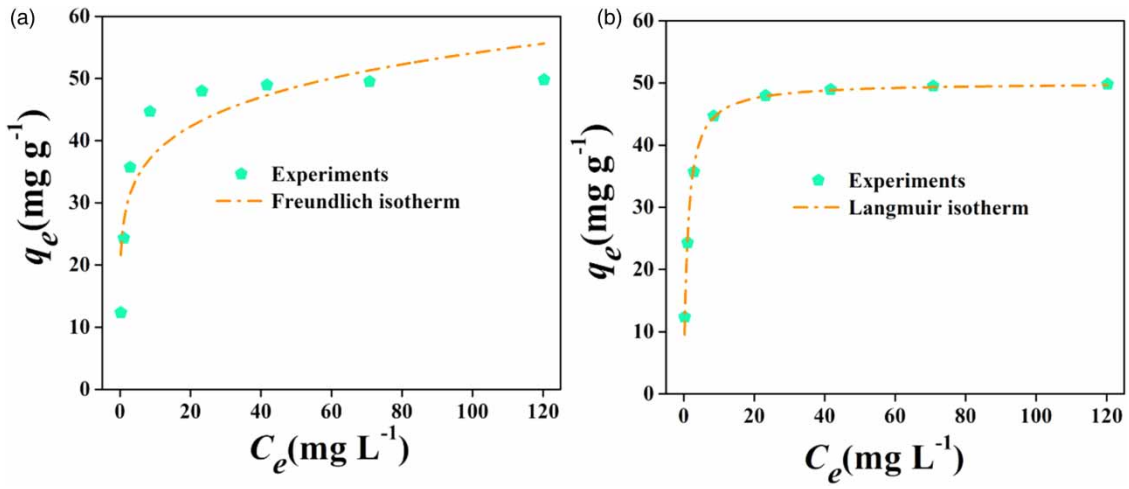

Figure 10 | Non-linear form of adsorption isotherms (a) Freundlich and (b) Langmuir.

conduction band. This excitation results in the formation of electron-hole pairs that bears the ability to delocalize throughout the crystal lattice of ZnO. Water molecules are split into H^+ ion and $OH^{\bullet}$ radical by holes while the electron reacts with oxygen molecules to generate superoxide ions. Further, these superoxide ions react with H^+ formed to give hydroperoxyl radicals ($H_2O^{\bullet}$). Two hydroperoxyl radicals yield hydrogen peroxide, which reacts with superoxide ions yielding hydroxyl free radicals. The oxidizing ability of these free radicals is very high. The attack of resulting hydroxyl radicals on adsorbed methylene blue dye molecules results in the rapid formation of degradation products via intermediate formation. The conversion of methylene blue dye into less harmful degradation products was traced back to the formation of active oxygen species (Figure S3, ESI). The photodegradation mechanism confirmed that in the due course of degradation process H_2O_2 is generated and combines with the superoxide ions. The resulting hydroxyl radical ($OH^{\bullet}$) breaks methylene blue into intermediates that further decompose to $CO_2 + H_2O$ (Ayodhya & Veerabhadram 2018). The stability and reusability of the CuBTC/ZnO chitosan composites were tested over methylene blue dye after recycling to replicate the experiments under identical conditions (Figure S4, ESI). More specifically, under sunlight irradiation, CuBTC/ZnO chitosan composites displayed sustained and consistent behaviour up to the 5th cycle (around 80%), which proves the composite's stability and recyclability.

4. CONCLUSIONS

This study reports the facile synthesis of CuBTC/ZnO chitosan composite beads and adsorption of methylene blue dye on it, followed by its photocatalytic regeneration. The SEM micrograph showed the nanoflower morphology of the ZnO and the octahedral units of CuBTC. The surface of the beads was rough and porous. XRD and the FT-IR spectra confirmed the structural properties of the CuBTC and ZnO nanoflowers. Further, the BET surface area of the CuBTC/ZnO chitosan composite beads was 5.91 $m^2\ g^{-1}$. The TGA analysis showed that incorporating ZnO imparts thermal stability to the composites. At pH 7, 1.6 g L^{-1} of the adsorbent gave a maximum adsorption capacity of 98.75% at the equilibration time of 90 min. The factors that governed these values were mainly the formation of NaCl during the adsorption process, decrease in the active sites on the adsorbent, and the aggregation of composites. The PSO models were found to best fit for the adsorption process. Of the Freundlich and the Langmuir models used to analyze the adsorption process, the Langmuir value was more useful, as was evident from the R^2 values. The Langmuir and PSO models' fitting indicated that the adsorption interaction between methylene blue and composites was chemisorption. It was clear from the mechanism that the role of chitosan is crucial in both the adsorption of methylene blue and in determining the kinetics of the process. The photocatalytic degradation was mainly due to ZnO, where the active oxygenated species were responsible for degrading the dye. The regeneration studies showed that the composites could be used up to 5 cycles without significant loss in the efficiency towards removing methylene blue.

ACKNOWLEDGEMENTS

The CSIR-CSMCRI PRIS number for this manuscript is 031/2022. The authors are grateful for partial funding support from the Council of Scientific and Industrial Research, India (MLP-0043). The authors acknowledge AED&CIF, CSMCRI for providing instrumental facilities. The authors also thank Ms Pratibha Yadav, IEHE Bhopal for help in synthesizing materials. The comments from anonymous reviewers and the editor have greatly improved the content.

CONFLICT OF INTEREST STATEMENT

We certify that the authors are not affiliated with or involved with any organization or entity with any financial interest or non-financial interest in the subject matter or materials discussed in this paper.

DATA AVAILABILITY STATEMENT

All relevant data are included in the paper or its Supplementary Information.

REFERENCES

Adeel, M., Saeed, M., Khan, I., Muneer, M. & Akram, N. 2021 Synthesis and characterization of Co–ZnO and evaluation of Its photocatalytic activity for photodegradation of methyl orange. *ACS Omega* **6** (2), 1426–1435.

Amode, J. O., Santos, J. H., Md. Alam, Z., Mirza, A. H. & Mei, C. C. 2016 Adsorption of methylene blue from aqueous solution using untreated and treated (Metroxylon spp.) waste adsorbent: equilibrium and kinetics studies. *International Journal of Industrial Chemistry* **7** (3), 333–345.

Arul, P. & Abraham John, S. 2017 Electrodeposition of CuO from Cu-MOF on glassy carbon electrode: a non-enzymatic sensor for glucose. *Journal of Electroanalytical Chemistry* **799**, 61–69.

Ayodhya, D. & Veerabhadram, G. 2018 A review on recent advances in photodegradation of dyes using doped and heterojunction based semiconductor metal sulfide nanostructures for environmental protection. *Materials Today Energy* **9**, 83–113.

Bangari, R. S., Yadav, A. & Sinha, N. 2021 Experimental and theoretical investigations of methyl orange adsorption using boron nitride nanosheets. *Soft Matter* **17** (9), 2640–2651.

Bangari, R. S., Yadav, A., Awasthi, P. & Sinha, N. 2022a Experimental and theoretical analysis of simultaneous removal of methylene blue and tetracycline using boron nitride nanosheets as adsorbent. *Colloids and Surfaces A: Physicochemical and Engineering Aspects* **634**, 127943.

Bangari, R. S., Yadav, A., Bharadwaj, J. & Sinha, N. 2022b Boron nitride nanosheets incorporated polyvinylidene fluoride mixed matrix membranes for removal of methylene blue from aqueous stream. *Journal of Environmental Chemical Engineering* **10** (1), 107052.

Biswal, H. J., Yadav, A., Vundavilli, P. R. & Gupta, A. 2021 High aspect ZnO nanorod growth over electrodeposited tubes for photocatalytic degradation of EtBr dye. *RSC Advances* **11** (3), 1623–1634.

Cai, H., Zhang, D., Ma, X. & Ma, Z. 2022 A novel ZnO/biochar composite catalysts for visible light degradation of metronidazole. *Separation and Purification Technology* **288**, 120633.

Cheng, J., Xuan, X., Yang, X., Zhou, J. & Cen, K. 2018 Preparation of a Cu(BTC)-rGO catalyst loaded on a Pt deposited Cu foam cathode to reduce CO2 in.a photoelectrochemical cell. *RSC Advances* **8** (56), 32296–32303.

Dindorkar, S. S., Patel, R. V. & Yadav, A. 2022 Quantum chemical study of the defect laden monolayer boron nitride nanosheets for adsorption of pesticides from wastewater. *Colloids and Surfaces A: Physicochemical and Engineering Aspects* **643**, 128795.

Hao, Y., Gao, Y., Gao, L., He, Y., Niu, Y., Hussain, S., Gao, R., Pfefferle, L. D., Shahid, M. & Wang, S. 2021 Amphiphilic core–shell magnetic adsorbents for efficient removal and detection of phthalate esters. *Chemical Engineering Journal* **423**, 129817.

Heidari, Z., Pelalak, R., Malekshah, R. E., Pishnamazi, M., Marjani, A., Sarkar, S. M. & Shirazian, S. 2021 Molecular modeling investigation on mechanism of cationic dyes removal from aqueous solutions by mesoporous materials. *Journal of Molecular Liquids* **329**, 115485.

Hu, Z., Peng, Y., Tan, K. M. & Zhao, D. 2015 Enhanced catalytic activity of a hierarchical porous metal–organic framework CuBTC. *CrystEngComm* **17** (37), 7124–7129.

Hussain, M. Z., Schneemann, A., Fischer, R. A., Zhu, Y. & Xia, Y. 2018 MOF derived porous ZnO/C nanocomposites for efficient dye photodegradation. *ACS Applied Energy Materials* **1** (9), 4695–4707.

Imran, M., Shaharoona, B., Crowley, D. E., Khalid, A., Hussain, S. & Arshad, M. 2015 The stability of textile azo dyes in soil and their impact on microbial phospholipid fatty acid profiles. *Ecotoxicology and Environmental Safety* **120**, 163–168.

Kellner-Rogers, J. S., Taylor, J. K., Masud, A. M., Aich, N. & Pinto, A. H. 2019 Kinetic and thermodynamic study of methylene blue adsorption onto chitosan: insights about metachromasy occurrence on wastewater remediation. *Energy, Ecology and Environment* **4** (3), 85–102.

Khoshhal, S., Ghoreyshi, A. A., Jahanshahi, M. & Mohammadi, M. 2015 Study of the temperature and solvent content effects on the structure of Cu–BTC metal organic framework for hydrogen storage. *RSC Advances* **5** (31), 24758–24768.

Kuwer, P., Yadav, A. & Labhasetwar, P. K. 2021 Adsorption of cupric, cadmium and cobalt ions from the aqueous stream using the composite of iron(II,III) oxide and zeolitic imidazole framework-8. *Water Science and Technology* **84** (9), 2288–2303.

Li, Y., Miao, J., Sun, X., Xiao, J., Li, Y., Wang, H., Xia, Q. & Li, Z. 2016 Mechanochemical synthesis of Cu-BTC@GO with enhanced water stability and toluene adsorption capacity. *Chemical Engineering Journal* **298**, 191–197.

Liu, J., Wang, Z., Bi, R., Mao, F., Wang, K., Wu, H. & Wang, X. 2020 A polythreaded Mn II-MOF and its super-performances for dye adsorption and supercapacitors. *Inorganic Chemistry Frontiers* **7** (3), 718–730.

Mahmoudzadeh, M., Fassihi, A., Emami, J., Davies, N. M. & Dorkoosh, F. 2013 Physicochemical, pharmaceutical and biological approaches toward designing optimized and efficient hydrophobically modified chitosan-based polymeric micelles as a nanocarrier system for targeted delivery of anticancer drugs. *Journal of Drug Targeting* **21** (8), 693–709.

Mariyam, A., Shahid, M., Mantasha, I., Khan, M. S. & Ahmad, M. S. 2020 Tetrazole based porous metal organic framework (MOF): topological analysis and dye adsorption properties. *Journal of Inorganic and Organometallic Polymers and Materials* **30** (6), 1935–1943.

Mohd Yusof, H., Abdul Rahman, N., Mohamad, R., Zaidan, U. H. & Samsudin, A. A. 2020 Biosynthesis of zinc oxide nanoparticles by cell-biomass and supernatant of Lactobacillus plantarum TA4 and its antibacterial and biocompatibility properties. *Scientific Reports* **10** (1), 19996.

Ndi Nsami, J. & Ketcha Mbadcam, J. 2013 The adsorption efficiency of chemically prepared activated carbon from cola Nut shells by on methylene blue. *Journal of Chemistry* **2013**, 1–7.

Oh, J.-W., Chun, S. C. & Chandrasekaran, M. 2019 Preparation and in vitro characterization of chitosan nanoparticles and their broad-spectrum antifungal action compared to antibacterial activities against phytopathogens of tomato. *Agronomy* **9** (1), 21.

Patel, R. V. & Yadav, A. 2022 Photocatalytic MIL101(Fe)/ZnO chitosan composites for adsorptive removal of tetracycline antibiotics from the aqueous stream. *Journal of Molecular Structure* **1252**, 132128.

Pattnaik, P., Dangayach, G. S. & Bhardwaj, A. K. 2018 A review on the sustainability of textile industries wastewater with and without treatment methodologies. *Reviews on Environmental Health* **33** (2), 163–203.

Peedikakkal, A. M. P. & Aljundi, I. H. 2020 Mixed-Metal Cu-BTC metal–organic frameworks as a strong adsorbent for molecular hydrogen at low temperatures. *ACS Omega* **5** (44), 28493–28499.

Rajak, R., Saraf, M., Mohammad, A. & Mobin, S. M. 2017 Design and construction of a ferrocene based inclined polycatenated Co-MOF for supercapacitor and dye adsorption applications. *Journal of Materials Chemistry A* **5** (34), 17998–18011.

Razavi-Khosroshahi, H., Edalati, K., Wu, J., Nakashima, Y., Arita, M., Ikoma, Y., Sadakiyo, M., Inagaki, Y., Staykov, A., Yamauchi, M., Horita, Z. & Fuji, M. 2017 High-pressure zinc oxide phase as visible-light-active photocatalyst with narrow band gap. *Journal of Materials Chemistry A* **5** (38), 20298–20303.

Schäfer, P., Kapteijn, F., van der Veen, M. A. & Domke, K. F. 2017 Understanding the inhibiting effect of BTC on CuBTC growth through experiment and modeling. *Crystal Growth & Design* **17** (11), 5603–5607.

Shahnawaz Khan, M., Khalid, M. & Shahid, M. 2020 What triggers dye adsorption by metal organic frameworks? *The Current Perspectives. Materials Advances* **1** (6), 1575–1601.

Shakoor, S. & Nasar, A. 2017 Adsorptive treatment of hazardous methylene blue dye from artificially contaminated water using cucumis sativus peel waste as a low-cost adsorbent. *Groundwater for Sustainable Development* **5**, 152–159.

Sharma, D. & Jha, R. 2017 Analysis of structural, optical and magnetic properties of Fe/Co co-doped ZnO nanocrystals. *Ceramics International* **43** (11), 8488–8496.

Shindhal, T., Rakholiya, P., Varjani, S., Pandey, A., Ngo, H. H., Guo, W., Ng, H. Y. & Taherzadeh, M. J. 2021 A critical review on advances in the practices and perspectives for the treatment of dye industry wastewater. *Bioengineered* **12** (1), 70–87.

Xu, W., Li, G., Li, W. & Zhang, H. 2016 Facile room temperature synthesis of metal–organic frameworks from newly synthesized copper/zinc hydroxide and their application in adsorptive desulfurization. *RSC Advances* **6** (44), 37530–37534.

Yadav, A. & Dindorkar, S. S. 2022 Adsorption behaviour of hexagonal boron nitride nanosheets towards cationic, anionic and neutral dyes: insights from first principle studies. *Colloids and Surfaces A: Physicochemical and Engineering Aspects* **640**, 128509.

Yadav, A., Patel, R. V., Labhasetwar, P. K. & Shahi, V. K. 2021a Novel MIL101(Fe) impregnated poly(vinylidene fluoride-co-hexafluoropropylene) mixed matrix membranes for dye removal from textile industry wastewater. *Journal of Water Process Engineering* **43**, 102317.

Yadav, A., Sharma, P., Panda, A. B. & Shahi, V. K. 2021b Photocatalytic TiO2 incorporated PVDF-co-HFP UV-cleaning mixed matrix membranes for effective removal of dyes from synthetic wastewater system via membrane distillation. *Journal of Environmental Chemical Engineering* **9** (5), 105904.

Yadav, A., Dindorkar, S. S. & Ramisetti, S. B. 2022a Adsorption behaviour of boron nitride nanosheets towards the positive, negative and the neutral antibiotics: insights from first principle studies. *Journal of Water Process Engineering* **46**, 102555.

Yadav, A., Patel, R. V., Singh, C. P., Labhasetwar, P. K. & Shahi, V. K. 2022b Experimental study and numerical optimization for removal of methyl orange using polytetrafluoroethylene membranes in vacuum membrane distillation process. *Colloids and Surfaces A: Physicochemical and Engineering Aspects* **635**, 128070.

Yadav, P., Yadav, A. & Labhasetwar, P. K. 2022c Sustainable adsorptive removal of antibiotics from aqueous streams using Fe_3O_4-functionalized MIL101(Fe) chitosan composite beads. *Environmental Science and Pollution Research* **198**.

Yaseen, D. A. & Scholz, M. 2019 Textile dye wastewater characteristics and constituents of synthetic effluents: a critical review. *International Journal of Environmental Science and Technology* **16** (2), 1193–1226.

Yedurkar, S., Maurya, C. & Mahanwar, P. 2016 Biosynthesis of zinc oxide nanoparticles using ixora coccinea leaf extract – a green approach. *Open Journal of Synthesis Theory and Applications* **05** (01), 1–14.

Zhang, M., Wang, L., Zeng, T., Shang, Q., Zhou, H., Pan, Z. & Cheng, Q. 2018 Two pure MOF-photocatalysts readily prepared for the degradation of methylene blue dye under visible light. *Dalton Transactions* **47** (12), 4251–4258.

Zhao, H., Xia, Q., Xing, H., Chen, D. & Wang, H. 2017 Construction of pillared-layer MOF as efficient visible-light photocatalysts for aqueous Cr(VI) reduction and dye degradation. *ACS Sustainable Chemistry & Engineering* **5** (5), 4449–4456.

First received 2 December 2021; accepted in revised form 15 April 2022. Available online 26 April 2022